Available online at www.sciencedirect.com
ScienceDirect
International Journal of Fatigue 30 (2008) 2050–2055
International Journal of Fatigue
www.elsevier.com/locate/ijfatigue

Technical note

The effect of machining on the surface integrity and fatigue life

Ataollah Javidi *, Ulfried Rieger, Wilfried Eichlseder

Department of Mechanical Engineering, University of Leoben, Franz-Josef-Straße 18, 8700 Leoben, Austria

Received 26 May 2007; received in revised form 4 December 2007; accepted 10 January 2008
Available online 26 January 2008

Abstract

Steel components often have to be machined after heat treatment in order to obtain the correct shape as well as the required surface finish. Surface quality influences characteristics such as fatigue strength, wear rate, corrosion resistance, etc. Hard turning allows manufacturers to simplify their processes and still achieve the desired surface finish quality. There are various parameters such as cutting speed, feed rate, and tool nose radius that are known to have a large impact on surface quality. This paper describes how feed rate and nose radius affect the surface integrity and fatigue life in turning. The results show that the effect of residual stress on fatigue life is more pronounced than the effect of surface roughness. The goal of this work is to identify a relationship between surface quality, turning process parameters and fatigue behavior of 34CrNiMo6.

Keywords: Surface integrity; Machining; Fatigue life

1. Introduction

The fatigue life of a machined part depends strongly on its surface condition. It has long been recognized that fatigue cracks generally initiate from free surfaces. This is due to the fact that surface layers experience the highest load and are exposed to environmental effects. Stress concentration, oxidation, and burning out of alloy elements (at high operational temperatures) are the factors acting upon the surface layers that contribute to crack initiation. Crack initiation and propagation, in most cases, can be attributed to surface integrity produced by machining [1]. The surface of a part has two important aspects that must be defined and controlled. The first aspect are geometric irregularities on the surface, and secondly the metallurgical alterations of the surface and the surface layer. This second aspect has been termed surface integrity. Field and Kahles [2] describe surface integrity as the relationship between surface geometric values and the physical properties such as residual stress, hardness and microstructure of the surface layers. Surface integrity influences the quality of the machined surface and subsurface, which both become extremely significant when manufacturing structural components that have to withstand high static and dynamic stresses. Tönshoff et al. [3] and several other authors [4–12] have reported how hard turning influences the surface integrity of a machined part [13]. Surface integrity was suggested to indicate the surface characteristics (microstructure, hardness, surface roughness, residual stress) that influence the part functionality. Among these characteristics, residual stresses play a key role. The residual stresses left by the turning operation depend both on the type of material being machined and on turning parameters [14]. There are various parameters such as cutting speed, feed rate, and tool nose radius that are known to have a large impact on surface quality [15–17]. Therefore it is important to gain better understanding how the finishing process affects the functional behavior of the machined parts. The goal of this work is to identify a relationship between surface integrity, turning process parameters and fatigue behavior of 34CrNiMo6.

* Corresponding author. Tel.: +43 3842 402 1403; fax: +43 3842 402 1402.
E-mail address: ataollah.javidi@mu-leoben.at (A. Javidi).

0142-1123/$ - see front matter © 2008 Elsevier Ltd. All rights reserved.
doi:10.1016/j.ijfatigue.2008.01.005

2. Material and experimental set-up

The material used for the cutting and fatigue life tests was a 0.34% carbon steel. Steel bars of the type 34CrNiMo6 (quenched and tempered) used in this investigation had been heat treated to obtain a tensile strength of 1100 MPa. The micrograph of the bar feedstock (cross-section A-A, Fig. 3) is presented in Fig. 1, which shows that the microstructure is composed of bainite. The chemical composition and mechanical properties of this steel are given in Table 1.

The test specimens were machined by turning in wet condition. Turning was performed using inserts DCMT 11 T3 02, 04, 08 4025 from Sandvik. The three inserts differ from each other in nose radius r_ε. An ordinary stable two-axes CNC lathe (Mori Seiki SL 25 2001) was used for longitudinal turning of the specimens. The cutting conditions employed for the samples are shown in Table 2.

Residual stresses were measured by means of the blind hole drilling method. The basic hole drilling procedure involves drilling a small hole into the surface of a component, at the center of a strain gauge rosette and measuring the relieved strains. The residual stresses originally present at the hole location are calculated from these strain values. In the hole drilling procedure, a three-element residual stress strain gauge rosette (EA-06-062RE-120 of MM series) is bonded to the surface of the specimen. The strain gauges are then connected to a suitable strain indicator. A hole drilling rig, which is shown in Fig. 2, was used for this purpose. It uses a small milling tool (about 1.6 mm diameter) mounted on an air turbine reaching a rotational speed of about 300,000 r/min. The drilling device is equipped with an optical microscope to accurately center

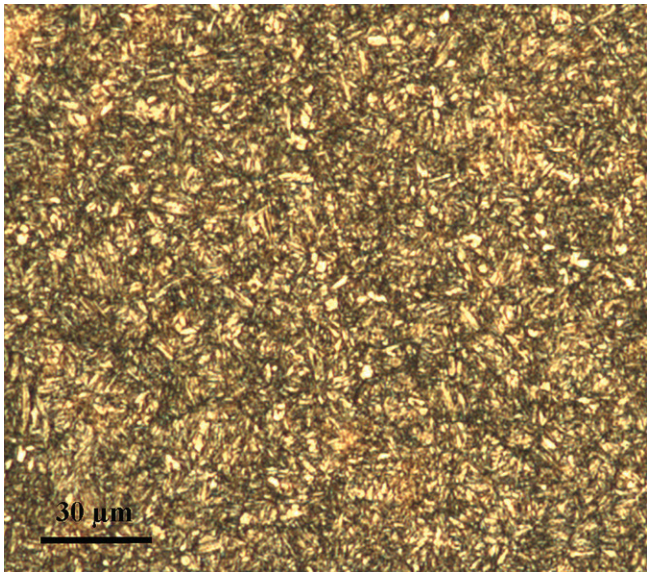

Fig. 1. Confocal scanning laser micrograph of the bar feedstock.

Table 1
Chemical composition and mechanical properties of 34CrNiMo6

Steel	Chemical composition (%)					Mechanical properties		
34CrNiMo6	C	Mn	Cr	Ni	Mo	R_e	R_m	A
	036	0.64	1.52	1.44	0.15	1085	1100	7.0

Table 2
Cutting conditions

Feed rate (mm/rev)	0.05, 0.1, 0.2, 0.3, 0.4
Nose radius (mm)	0.2, 0.4, 0.8
Depth of cut (mm)	0.5
Cutting speed (m/min)	80

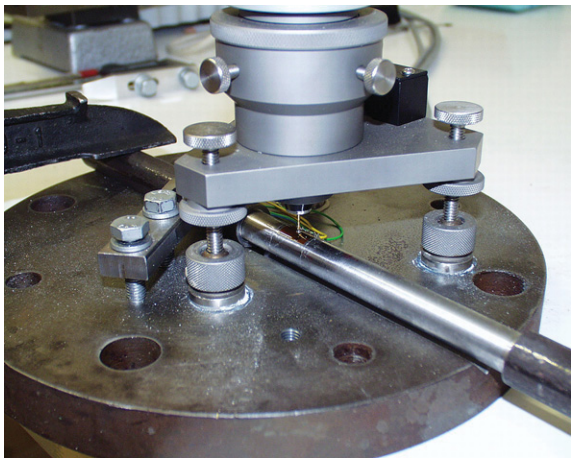

Fig. 2. Hole drilling rig.

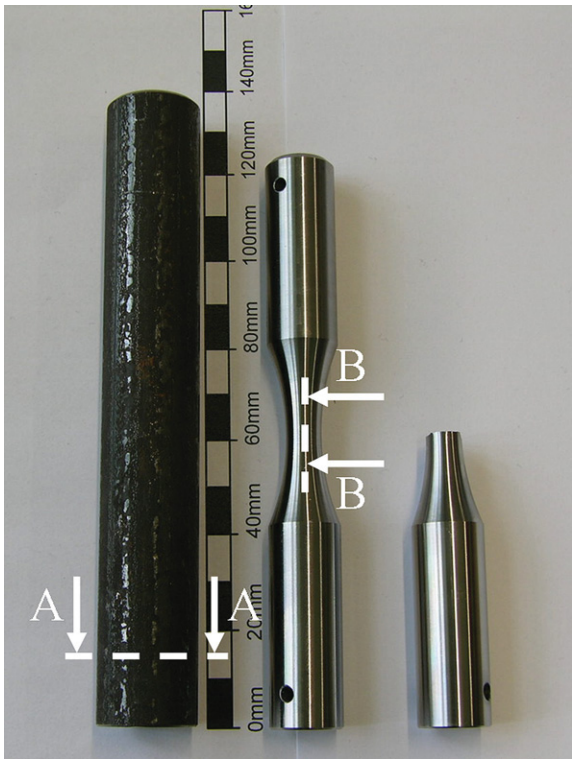

Fig. 3. Bar feedstock and fatigue test specimen.

the hole in the middle of the rosette. Depth increments of 127 μm were used in the near-surface layer. For each incremental step, the strains were acquired until the variation with depth become constant. The holes were drilled to a depth of about 1.27 mm.

Nose radius of the tool and feed rate were varied for this investigation. The microhardness, surface roughness and residual stress of the specimens were measured before the fatigue life test. Fig. 3 shows the configuration of the bar feedstock and fatigue test specimen before and after test.

3. Results and discussion

3.1. Metallographic examination of machined surface

Machining influences the conditions of the subsurface microstructure, which was examined under a confocal scanning laser microscope (LEXT) in etched condition. Selections of the etched subsurface microstructures generated during cutting are illustrated in Fig. 4 and Fig. 5. Fig. 4 illustrates the LEXT longitudinal-sectional viewgraph (marked as B–B, in Fig. 3) with a very thin localized plastic deformation zone of about 3–4 μm while using different feeds and nose radii with the same cutting speed as given in Table 2.

A scanning electron microscope image (SEM, Fig. 5) of the layer underneath the machined surface shows that the grain boundaries tend to deform in the direction of feed due to the high temperature and force generated during hard turning. Region A indicates that the original grains are no longer discernible. Clearly, the above observations indicate that high plastic deformation was generated after machining.

3.2. Microhardness analysis of the produced surface

In order to identify more clearly the extent of the alterations in the subsurface microstructure, the change of the subsurface microhardness was measured with an automated microhardness tester (Fischerscope® H100C) equipped with a Vickers indenter and a continuously applied load of 100 mN. The device measures the universal hardness according to ISO 14577. Fig. 6 shows the indentation arrangement at different positions beneath the machined surface. Fig. 7 details the variation of the

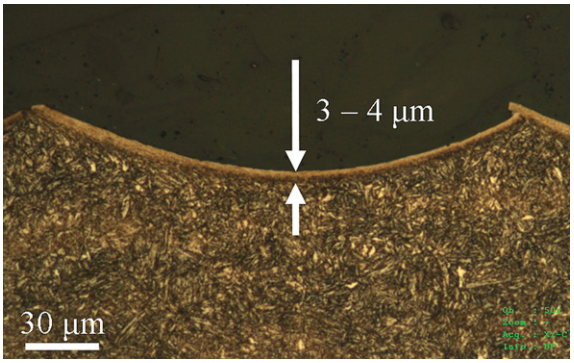

Fig. 4. Localized plastic deformation zone beneath machined surface.

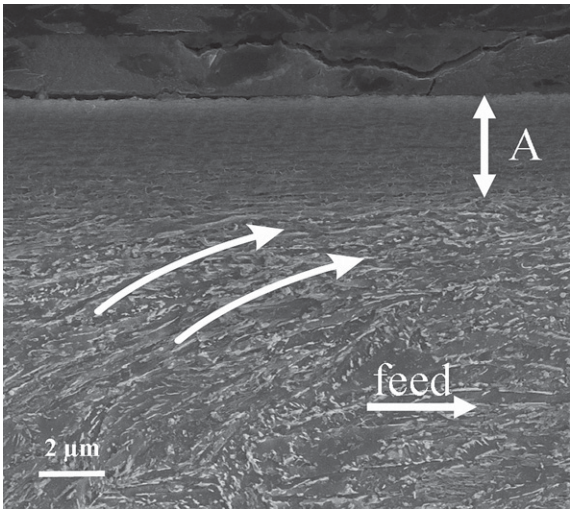

Fig. 5. SEM image of the layer underneath the machined surface.

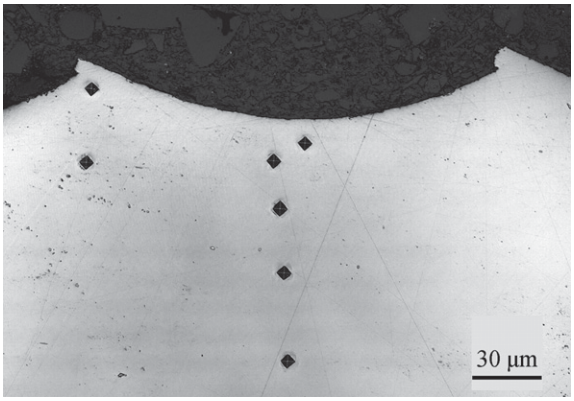

Fig. 6. Indentation arrangement beneath the machined surface ($f = 0.2$, $r_\varepsilon = 0.2$).

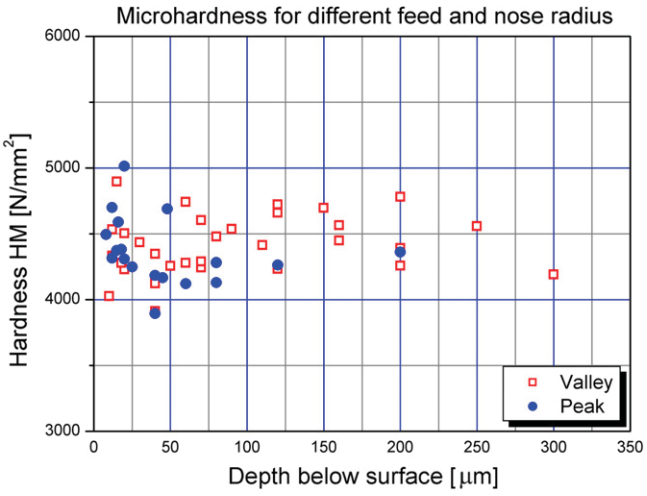

Fig. 7. Microhardness variations beneath the machined surface.

microhardness with the depth beneath the machined surface produced by different cutting conditions as shown in Table 2. The analysis of the results presented in Fig. 7 shows that there is no significant variation in hardness.

3.3. Surface roughness measurements

The surface roughness of the machined part is largely determined by the feed and tool nose radius. A large feed will give shorter cutting times but a poor surface finish. A large nose radius will generate a better surface finish but an excessively large nose radius can lead to vibration tendencies, unsatisfactory chipbreaking and shorter tool-life because of insufficient cutting edge engagement. In practice, therefore, the size of the insert nose radius and the feed may be limited in an operation. The geometric contribution of tool nose radius and tool feed, shown in Fig. 8, is also called theoretical surface roughness. A basic theoretical model for surface roughness is approximated by the following equation:

$$R_{\max} = \frac{f^2}{8 \times r_\varepsilon} \tag{1}$$

where f is feed rate (mm/rev.) and r_ε is the tool nose radius (mm).

According to this model, one needs only to decrease the feed rate or to increase the tool nose radius to improve desired surface roughness. Tool vibration and chip adhesion are such effects that lead to the degradation of surface roughness in this model. After the turning operation, the part surface finish was measured using laser scanning microscopy. Fig. 9 shows a 3D topographic map of the machined surface. In this investigation, the part surface finish was assessed by means of the surface roughness parameter $R_{\max}$. A schematic description of this parameter for an arbitrary machined surface is shown in Fig. 10.

Note that $R_{\max}$ (the maximum height of roughness) describes the sum of the maximum peak height R_p and the maximum valley depth R_v of the contour curve at the reference length. The experimental investigation was performed using different nose radii and feed rates. The surface roughness measurements were repeated at least five times for each specimen. Fig. 11 shows that the actual surface roughness does not match the theoretical surface roughness and Eq. (2) describes the relationship between real and theoretical surface roughness for the cutting conditions from Table 2:

$$R_{\max(\text{real})} = 1.14 \times R_{\max(\text{Theoretical})} + 0.3 \tag{2}$$

Fig. 12 illustrates the effect of the nose radius on the surface roughness for the cutting condition employed for the fatigue test ($f = 0.2$, $r_\varepsilon = 0.2$, 0.4, 0.8). The results present that the value of $R_{\max}$ parameter obtained for the samples increases with decreasing the nose radius (r_ε).

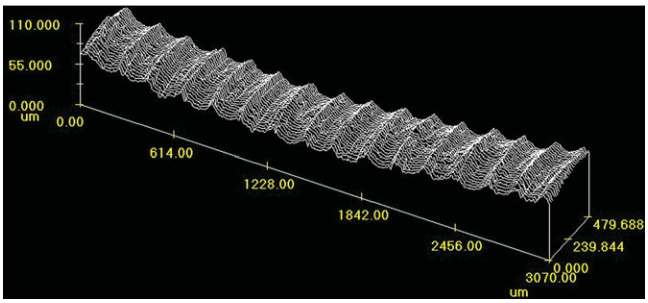

Fig. 9. 3D topographic map of machined surface.

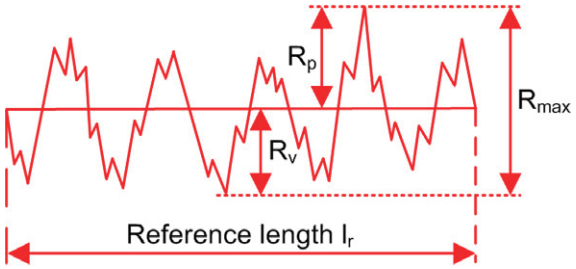

Fig. 10. A schematic illustraion of surface roughness parameter, $R_{\max}$.

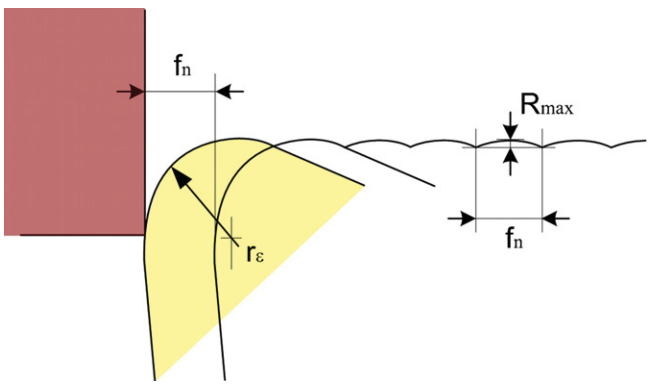

Fig. 8. Illustration of roughness on the finished surface.

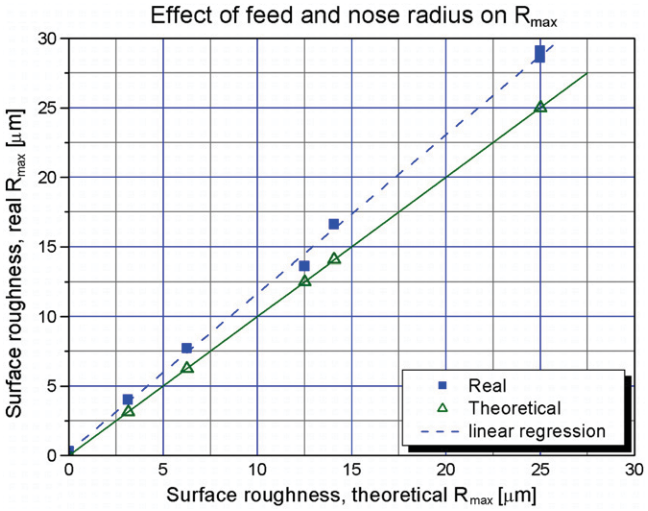

Fig. 11. Real and theoretical surface roughness.

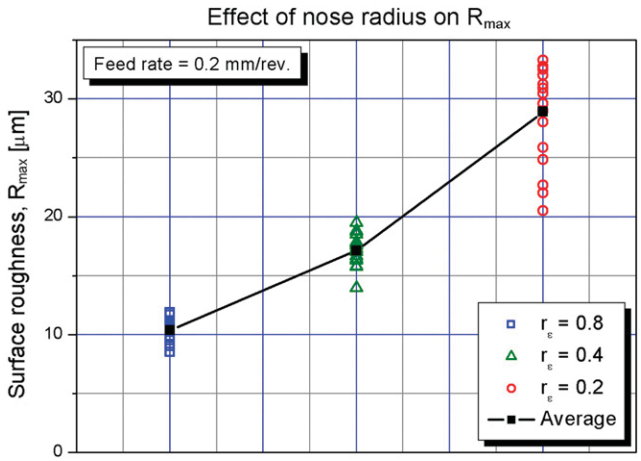

Fig. 12. Effect of nose radius on R_{max}, feed rate = 0.2 mm/rev.

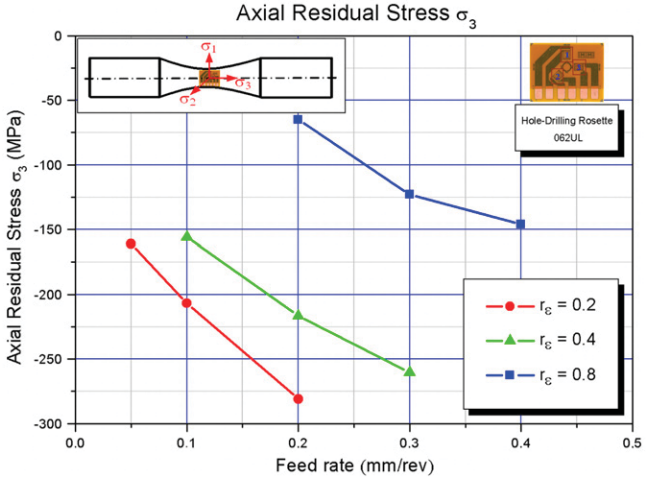

Fig. 14. Axial residual stress σ_3 versus feed rate.

3.4. Residual stress measurements

After the turning operation, the residual stresses were measured using the blind hole drilling method. The machining of round samples was carried out with different feed rates f and nose radii r_ε. Fig. 13 shows the distribution of the residual stress of the machined surface measured by this method. Measurements were taken along the circumference and axial directions. Residual stress along the axial direction was expected to affect the rotating bending fatigue life of the specimens. In this study, the integral method is examined as a procedure for determining non-uniform residual stress fields using strain relaxation data from the hole drilling method. In the integral method, the contributions of the total measured strain relaxations at all depths are considered simultaneously and this provides an evaluation of residual stress within each increment of depth. A description of this method can be found in Schajer [18]. Figs. 14 and 15 show the average value of stresses over a depth range from 0 to 0.127 mm for specimens with different process parameters. All occurring stresses are compressive. It can be seen that an increase of feed rate causes an increase of compressive stresses in both directions. On the other hand, an increase of the nose radius of the insert causes a decrease of the compressive residual stresses.

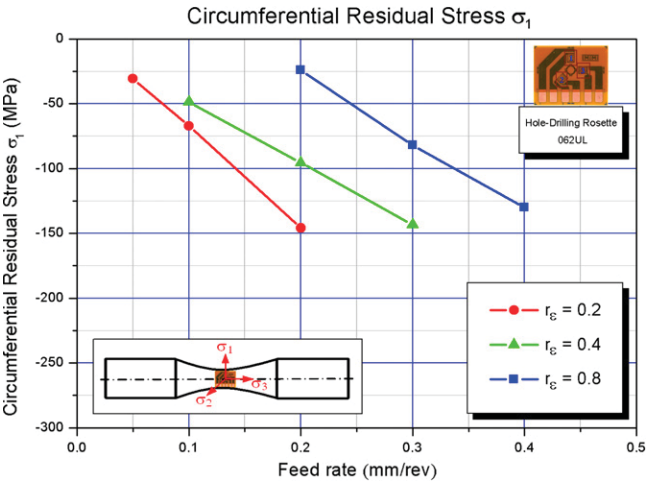

Fig. 15. Circumferential residual stress σ_1 versus feed rate.

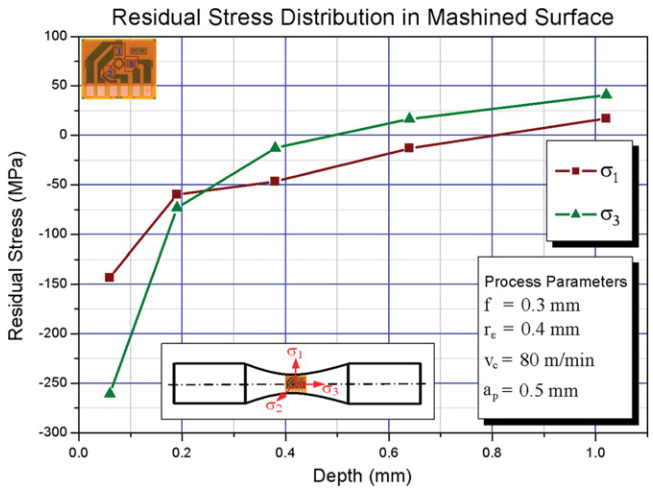

Fig. 13. Residual stress distribution in machined surface.

4. Influences on fatigue life

The rotating bending fatigue tests that were performed on the test specimens as per the cutting conditions shown in Table 3. Rotation speed was 3800 rev/min. At least sixteen specimens were used to verify the fatigue life for every combination of feed and nose radius. When the number of

Table 3
Cutting condition employed for fatigue test

Feed rate (mm/rev)	0.2
Nose radius (mm)	0.2, 0.4, 0.8
Depth of cut (mm)	0.5
Cutting speed (m/min)	80

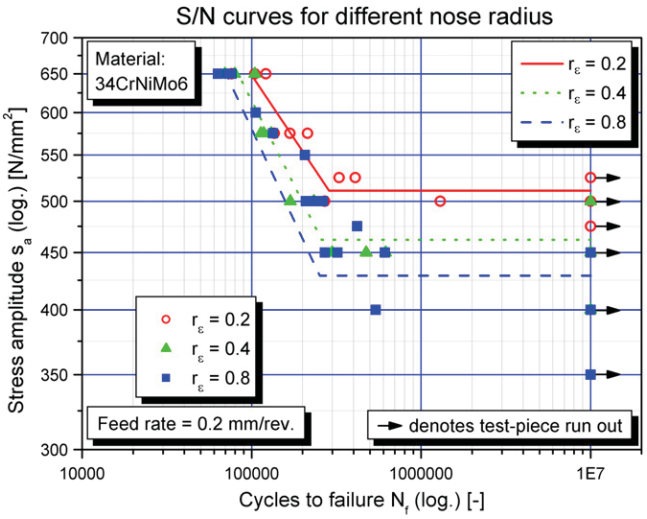

Fig. 16. Fatigue life of turned specimens with different nose radius.

rotation exceeded 10^7 the test was stopped, which means the test specimen will not break under that condition (test-piece run out). Fig. 16 shows the relationship between cutting condition and fatigue life. Although the surface roughness of specimens with $r_\varepsilon = 0.2$ is higher than turned specimens with $r_\varepsilon = 0.4$ and 0.8, the results show that the specimens with a nose radius of $r_\varepsilon = 0.2$, have a higher fatigue life than specimens with 0.4 and 0.8 mm nose radius. That means a higher compressive residual stress causes a higher fatigue life and the effect of residual stress on fatigue life is more than the effect of surface roughness.

5. Conclusion

This work presents an experimental study on the relationship between surface integrity, turning process parameters and fatigue behavior of 34CrNiMo6. The following conclusions can be drawn:

- The plastic deformation of the grain boundaries was found at the first 3–4 μm of the subsurface layer after machining.
- No significant variation in hardness was observed beneath the machined surface produced by different cutting conditions.
- Surface roughness at the same feed rate becomes higher when a small nose radius is used.
- The residual stress induced by the turning process tends to become more compressive as the feed rate increases. On the other hand, an increase of the nose radius of the insert causes a decrease of the compressive residual stresses. Thus it is evident that the feed rate and nose radius are the key parameters that control residual stress in turning.
- It can be seen that an increase of compressive residual stress causes an increase of fatigue life.

Acknowledgements

This work was supported by the Austrian Aeronautics Research. The authors would like to thank Robert Schreiber and his team (Pankl Drivetrain Systems GmbH) for the support in sample machining.

References

[1] Zahavi E, Torbilo V. Fatigue design – life expectancy of machine parts. CRC Press; 1996.
[2] Field M, Kahles J. Review of surface integrity of machined components. Ann CIRP 1971;20:153–63.
[3] Tönshoff HK, Arendt C, Ben Amor R. Cutting of hardened steel. Ann CIRP 2000;49(2):547–66.
[4] Liu CR, Mittal S. Optimal pre-stressing the surface of a component by superfinish hard turning for maximum fatigue life in rolling contact. Wear 1998;219:128–40.
[5] Matsumoto Y, Hashimoto F, Lahoti G. Surface integrity generated by precision hard turning. Ann CIRP 1999;48:59–62.
[6] Jacobson M. Surface integrity of hard-turned M50 steel. Proceedings of the Institution of Mechanical Engineers Part B J Eng Manuf 2002;216(1):47–54.
[7] Jacobson M, Patrik D, Fredrik G. Cutting speed influence on surface integrity of hard turned bainite steel. J Mater Proc Technol 2002;128(1–3, 6):318–23.
[8] Thiele JD, Melkote SN. Effect of cutting edge geometry and workpiece hardness on surface generation in the finish hard turning of AISI 52100 steel. J Mater Proc Technol 1999;94:216–26.
[9] Brinksmeier E, Cammett JJ, Leskovar P, Peters J, Tönshoff HK. Residual stresses-measurements and causes in machining processes. Ann CIRP 1982;31:491–510.
[10] Vomacka P., Walburger H., Residual stresses due to hardmachining industrial experiences, In: Proceedings of the 5th European conference on residual stresses, Switzerland, 2000, p. 592–97.
[11] König W, Berktold A, Koch K-F. Turning versus grinding: a comparison of surface integrity aspects and attainable accuracies. Ann CIRP 1993;42:39–43.
[12] Tönshoff H.K., Wobker H.-G., Brandt D., Potential and limitation of hard turning, SME Tech. Papers, 1995. p. MR95–MR215.
[13] Gunnberg F, Escursell M, Jacobson M. The influence of cutting parameters on residual stresses and surface topography during hard turning of 18MnCr5 case carburised steel. J Mater Proc Technol 2006;174:82–90.
[14] Capello E. Residual stresses in turning part I: influence of process parameters. J Mater Proc Technol 2005;160:221–8.
[15] Dahlman P, Gunnberg F, Jacobson M. The influence of rake angle, cutting feed and cutting depth on residual stresses in hard turning. J Mater Proc Technol 2004;147:181–4.
[16] Arola D, Williams CL. Estimating the fatigue stress concentration factor of machined surface. Int J Fatigue 2002;24:923–30.
[17] Sasahara H. The effect on fatigue life of residual stress and surface hardness resulting from different cutting conditions of 0.45%C steel. J Mach Tool Manuf 2005;45:131–6.
[18] Schajer GS. Measurement of non-uniform residual stresses using the hole drilling method, part I – stress calculation procedures. ASME J Eng Mater Technol 1988;110:338–43.